minerals

MDPI

Article

Mineral Chemistry of Pyrochlore Supergroup Minerals as Records of Nb Mineralization Processes in NYF-Type Pegmatites: A Case Study of the Emeishan Large Igneous Province, SW China

Rong Yin [1,2,*], Xiaoming Sun [1,2,3], Shengwei Wang [4] and Bin Wu [5]

[1] School of Earth Sciences and Engineering, Sun Yat-sen University, Guangzhou 510275, China
[2] Guangdong Provincial Key Laboratory of Geodynamics and Geohazards, Guangzhou 510275, China
[3] School of Marine Sciences, Sun Yat-sen University, Guangzhou 510006, China
[4] Chengdu Institute of Geology and Mineral Resources, China Geological Survey, Chengdu 610081, China
[5] State Key Laboratory of Nuclear Resources and Environment, East China University of Technology, Nanchang 330013, China
* Correspondence: yinr6@mail.sysu.edu.cn

Abstract: Alkaline igneous rocks have become a potentially important source of Nb, except for the carbonatites. The metallogenetic mechanism of Nb during the magmatic-hydrothermal evolution of alkaline rocks remains ambiguous. From the perspective of Nb minerals, the mineral chemistry of pyrochlore supergroup minerals provides the mineralogical evidence for indicating the respective contributions of magma and hydrothermal fluids to Nb mineralization. In the Miyi County of the Panzhihua-Xichang (Pan-Xi) area, the central zone of the Permian Emeishan large igneous province (ELIP) in SW China, hundreds of Nb-Y-F mineralized pegmatites (NYF-type) are exposed. This study conducted in situ mineral chemistry analyses on four types of pyrochlores to elucidate the Nb mineralization process. Both Pcl-I and Pcl-II exhibit well-developed oscillatory zoning (OZ), representing magmatic pyrochlore formed through disequilibrium crystallization in an oscillatory environment. Pcl-III, with a homogeneous and less variable composition, is also considered of magmatic origin due to its coherent chemical evolution with Pcl-II. Pcl-IV is considered of hydrothermal origin based on its irregular zoning texture, extremely high Na_2O contents, and compositional gap compared with magmatic types. The decrease in TiO_2 contents, coupled with the increase in Na_2O, F, and Nb_2O_5 contents from Pcl-I to Pcl-III and from the core to the rim of zoned Pcl-II, indicates that fractional crystallization facilitates the crystallization of albite and the enrichment of volatiles, as well as the precipitation of Nb from the early to late stages. During the magmatic-hydrothermal transition stage, the reductive, Na- and F-enriched fluid transports Nb more effectively, leading to further Nb enrichment in pyrochlore. Consequently, there are two-stage Nb mineralization processes associated with the magmatic-hydrothermal evolution in the Miyi pegmatite, with the primary magmatic ore assemblages being the dominant Nb mineralization, which may be a general model for the mineralization of NYF-type pegmatites.

Keywords: NFY-pegmatite; pyrochlore; Nb mineralization; magmatic-hydrothermal evolution; Emeishan large igneous province; SW China

check for updates

Citation: Yin, R.; Sun, X.; Wang, S.; Wu, B. Mineral Chemistry of Pyrochlore Supergroup Minerals as Records of Nb Mineralization Processes in NYF-Type Pegmatites: A Case Study of the Emeishan Large Igneous Province, SW China. *Minerals* **2024**, *14*, 13. https://doi.org/10.3390/min14010013

Academic Editor: Jiří Sejkora

Received: 20 November 2023
Revised: 14 December 2023
Accepted: 17 December 2023
Published: 21 December 2023

Copyright: © 2023 by the authors. Licensee MDPI, Basel, Switzerland. This article is an open access article distributed under the terms and conditions of the Creative Commons Attribution (CC BY) license (https://creativecommons.org/licenses/by/4.0/).

1. Introduction

Niobium is a critical material widely utilized in modern society characterized by its applications in high-tech industries [1,2]. The majority of economically significant Nb deposits are associated with carbonatites, which contain more than 50% of global Nb resources [2]. Besides the carbonatites, alkaline igneous rocks are emerging as a potentially vital source of Nb; for instance, Nb is currently being mined in the Lovozero layered alkaline igneous complex in the Kola peninsula in Russia, the Motzfeldt layered complex

in Greenland, and the Nechalacho layered intrusive suite and the Strange Lake alkaline pegmatite in Canada, etc. [2].

The upwelling mantle plume may generate voluminous alkaline magma, potentially containing large Nb deposits [3,4]. The rise of the late Permian mantle plume in southwest China formed the Emeishan large igneous province (ELIP) comprising extensive continental flood basalt, mafic-ultramafic intrusions, and alkaline rocks [5–11]. In the Panzhihua-Xichang (Pan-Xi) area, the central zone of the ELIP, hundreds of syenitic and pegmatitic dikes contain most of the Nb resources in the ELIP, formed in 257–259 Ma [12,13]. These pegmatites are Nb-Y-F mineralized and could be classified as NFY-type pegmatites [13–15]. The reconstruction of Nb metallogenic mechanisms in NYF-type pegmatites in the ELIP provides an opportunity to understand the potential for mineralization related to the mantle plume.

The main issue of Nb mineralization in alkaline rocks is whether the minerals hosting Nb crystallized directly in magma or when the hydrothermal fluids remobilized during the magmatic-hydrothermal transitional processes. Solubility experiments of Nb-Ta oxide minerals, including columbite-group minerals, pyrochlore, and microlite, suggest that Nb mineralization occurs during the fractionation of alkaline melts [16–19]. Mineralogical features such as the presence of vein-like columbite in the Bailongshan pegmatite [20] and re-precipitated pyrochlore in the dissolved titanite in the Fangcheng syenite [21] indicate hydrothermal overprinting of magmatic Nb mineralization. Thus, the key factor controlling Nb mineralization remains poorly understood.

Pyrochlore supergroup minerals are common Nb-dominant minerals in NYF-type pegmatites characterized by the general formula $A_{2-m}B_2X_{6-w}Y_{1-n}{\cdot}pH_2O$, where m = 0–1.7, w = 0–0.7, n = 0–1, and p = 0–2. The A-site can be occupied by Na, Ca, Sr, Ba, Sc, Y, REE, U, Th, Pb, □ (□ stands for a vacancy), or H_2O; the B-site atoms mainly include Nb, Ta, Ti, Sb, W, but also V, Zr, Fe, Al, and Si; the X-site is O, OH^-, and F; and the Y-site is OH^-, F, O, K, Rb, Cs, H_2O, and □ [22–24]. The chemistry of pyrochlore supergroup minerals could be utilized as an optimal tracker of Na, Ca, REE, and Nb changes in melt or fluid, as well as volatiles (including F and H_2O) for changes in the metallogenic environment, which have been proven to decipher details of the crystallization environment, equilibrium melt properties, and magmatic-hydrothermal transition processes in alkaline rocks [23,25–30]. In this study, the detailed textural and chemical evolution of pyrochlore supergroup minerals in the NYF-type pegmatite in the Pan-Xi area are used to elucidate the specific roles of magmatic-hydrothermal evolution in Nb mineralization, providing insights into the source and metallogenic mechanism of Nb in plume-related NFY-type pegmatites.

2. Geological Background

The ELIP is located at the western edge of the Yangtze craton near the boundary with the Songpan-Ganze terrane in southwestern China (Figure 1a). The Yangtze craton comprises Meso-Proterozoic granitic gneisses and metasedimentary rocks intruded by Neoproterozoic (~800 Ma) granites and mafic rocks [31,32]. Overlying the Neoproterozoic granites are a series of marine and terrestrial strata from the late Neoproterozoic (~600 Ma) to the Permian [33]. A late Permian (~260 Ma) mantle plume origin for the ELIP is accepted as suggested by several geological, geochemical, and geophysical studies [5,7,34,35]. Most of the ELIP magmas (~85%) erupted 1.45 ± 0.5 million years ago [36]. The ELIP consists primarily of continental flood basalts (including low-Ti and high-Ti groups) and pyroclastic rocks covering an area of approximately ~7×10^5 km^2. The thickness of the Emeishan volcanic succession varies from over five kilometers in the west to several hundred meters in the east [37,38]. The ELIP can be divided into inner, intermediate, and outer zones based on the amounts of surface uplift and erosion [5]. High-Ti basalts are exposed in both the inner and outer zones, while the low-Ti group is predominantly located in the inner zone [7].

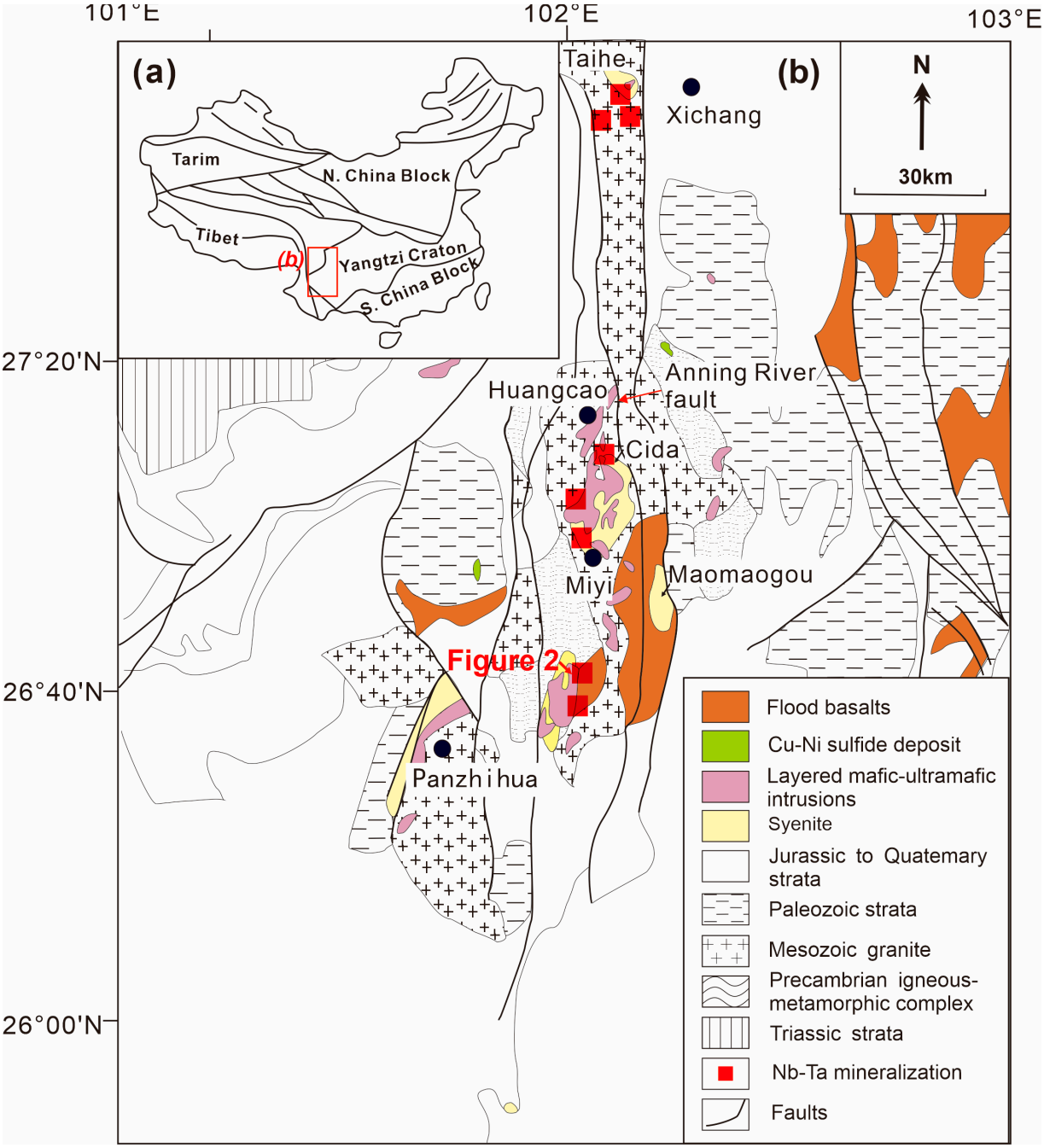


Figure 1. Simplified geological map of (**a**) China and (**b**) the Pan-Xi area (modified by [5,12]).

The Panzhihua-Xichang (Pan-Xi) area, located in the inner zone of the ELIP, extends over a distance of ~700 km [39]. In the Pan-Xi area, massive igneous complexes developed from north to south along the NS-trending Anninghe fault zone (Figure 1b). These complexes commonly consist of temporally and spatially correlated layered mafic/ultramafic intrusions, felsic intrusions, and a small volume of continental flood basalts [8,11,37,38,40]. Several large mafic/ultramafic intrusions host giant V-Ti-Fe oxide deposits (e.g., Panzhihua, Hongge, Baima, and Taihe) [41,42]. Additionally, some small intrusions contain Ni-Cu-PGE sulfide deposits (e.g., Yangliuping, Limahe, and Jinbaoshan) [11,42,43]. The felsic intrusions include amphibole/quartz/nepheline syenite and granites, named from north to south as Taihe, Cida, Miyi, and Ailanghe, etc. (Figure 1b) [10]. It is suggested that these syenites and granites represent the very late stage of the Emeishan plume activity since they always intrude on the adjacent basalts and mafic/ultramafic intrusions in the

field [10]. The majority of the syenites and granites are chemically peralkaline and display A-type granitic characteristics, while a minority exhibit peraluminous features and I-type granite characteristics [6,8,38,44]. The A-type granites were formed in ~260 Ma, based on high-precision zircon SHRIMP U–Pb dating [8]. It is further proposed that these A-type granites are derived from the differentiation of Emeishan high-Ti basalt [6,38,44]. The I-type granite was derived from the partial melting of Mesoproterozoic basement rocks of the Yangtze Block [8,44].

In the Pan-Xi area, hundreds of syenitic and pegmatitic dikes surround the felsic intrusions and intrude the mafic/ultramafic intrusions (Figure 2) [12]. They host the majority of Nb-Ta ore deposits in the region, delineating over 30 ore bodies in the Xichang, Dechang, Huili, Huidong, and Miyi areas (Figure 1b) [15]. For example, the Baicao and Luku Nb deposits (syenitic dyke-hosted) contain an estimated resource of 465 and 30 metric tonnes (t) of Nb_2O_5 and Ta_2O_5, respectively (Figure 2) [12].

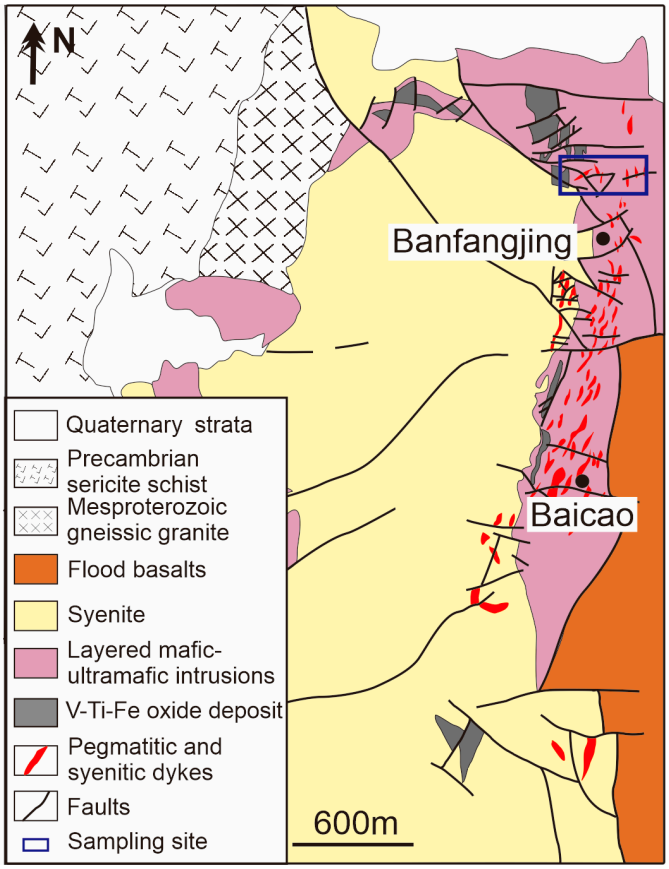


Figure 2. Simplified geologic map showing the relationship between pegmatitic and syenitic dykes with the layered mafic-ultramafic and felsic intrusions in ELIP (modified by [12]), and the prospected locations of the Miyi pegmatite.

Apart from syenitic dykes, recently discovered alkaline pegmatites classified as NFY-type in Miyi County exhibit high Nb and REEs ore grades, with maximum values reaching up to 0.4% Nb_2O_5 and 0.5% total REE oxides (Figure 2) [13]. The Miyi pegmatites comprise dozens of aplite and pegmatite dikes that intrude on the layered mafic-ultramafic intrusion-hosted Zhujiabaobao Fe-Ti-V oxide deposits (Figure 3a). The dendritic pegmatites extend 20–1500 m in length and are 0.3–5 m wide [13]. The Miyi pegmatite, formed around ~258 Ma as determined by LA-ICP-MS U-Pb dating of zircons [13], exhibits positive $\varepsilon_{Hf}(t)$ values of zircons (ranging from 1.5 to 9.1) [13], indicating its plume-related origin and possible derivation from magma resembling A-type granites in the ELIP.

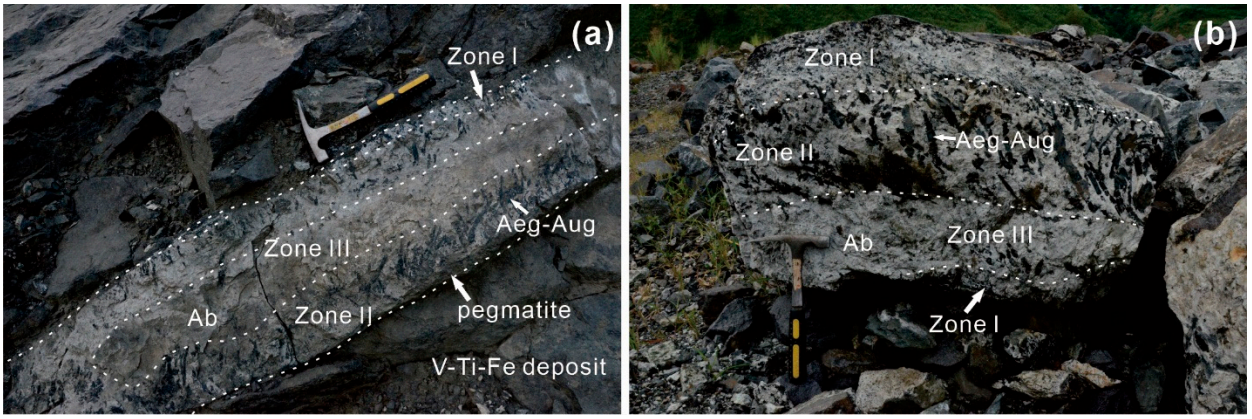


Figure 3. Field photograph of (**a**) the white to light grey Miyi pegmatite intruding in the deep grey V-Ti-Fe oxide deposit, (**b**) the textural zones of the Miyi pegmatite, including the border (Zone I), intermediate (Zone II), and core (Zone III). Abbreviations: Ab, albite; Aeg-Aug, aegirine-augite.

The rock-forming minerals of the Miyi pegmatites are aegirine-augite, albite, plagioclase, K-feldspar, and biotite (Figure 3), along with accessory minerals such as zircon, titanite, apatite, ilmenite, and fluorite [13]. The Miyi pegmatite displays asymmetrical zoning in its internal structure (Figure 3). Three textural zones can be identified outside-to-inside based on the variations in petrological texture and mineral assemblages: border zone (Zone I), intermediate zone (Zone II), and inner zone (Zone III) (Figure 3). A contact zone composed of biotite aggregates with a width of ~1 cm is observed at the boundary between the pegmatite and Fe-Ti-V oxide deposits [13]. The grain sizes of rock-forming minerals progressively increase from Zone I to Zone II, with the crystal length of aegirine-augite notably increasing from ~1 cm to ~30 cm (Figure 3). Biotite and aegirine-augite are absent in Zone III, and blocky albite dominates the mineral assemblage (Figure 3). Pegmatite exhibits Nb mineralization in all textural zones, with the mineralization of REE mainly occurring in Zone II [13].

3. Samples and Analytical Methods

Twenty samples were collected from all textural zones in the Miyi pegmatite. Polished thin sections of these samples were prepared for petrographic observations and the quantitative determination of pyrochlore mineral chemistry.

Preliminary petrographic observations were conducted using a ZEISS AXIO microscope (Carl Zeiss AG; Oberkochen, Baden-Württemberg, Germany) under both transmitted and reflected light conditions. Mineralogical identification and back-scattered electron (BSE) images were obtained using a TESCAN MIRA (TESCAN; Brno, Czechia) field emission scanning electron microscope (FE-SEM) equipped with energy dispersive spectroscopy (EDS) at the School of Marine Sciences, Sun Yat-sen University (SYSU).

The chemical composition of pyrochlore in the Miyi pegmatite was quantified using a JEOL JXA-8530F Plus (JEOL Ltd.; Akishima, Tokyo, Japan) field emission-electron probe microanalyzer (FE-EPMA) equipped with five wavelength-dispersive spectrometers at the State Key Laboratory of Nuclear Resources and Environment, East China University of Technology. The operating conditions included an accelerating voltage of 15 kV, a beam current of 20 nA, and a beam diameter of ~3 μm. Peak counting times were 10 s for major elements, 20 s for minor elements, and 10 s for volatile species (Na, K, and F). The following natural and synthetic standards were used for analytical standards: apatite (Ca), jadeite (Na), topaz (F), rutile (Ti), Ta metal (Ta), Nb metal (Nb), monazite (La, Ce, Pr, Nd), synthetic REE-bearing phosphate mineral (Sm), YAG (Y), uraninite (U, Th, Pb), plagioclase (Al), zircon (Zr, Si), magnetite (Fe), rhodonite (Mn), barite (Ba), and pyroxene (Mg). The ZAF routine was used for data reduction. The detection limits for most minor elements are approximately 200–300 ppm. X-ray elemental mapping was performed on the

FE-EPMA to identify the chemical heterogeneities and spatial distribution of elements in single pyrochlore crystals. The mapping used an accelerating voltage of 15 kV and a beam current of 40 nA.

4. Results

4.1. Mineralogical Features of Pyrochlore Supergroup Minerals

The pyrochlore supergroup minerals commonly present in Zones I and II in the Miyi pegmatite are further classified into four distinct types based on their internal textures and chemical compositions.

Type I pyrochlore supergroup minerals (Pcl-I) are present in Zone I. They are euhedral to subhedral, ranging from 20 to 500 μm across, and occur interstitially within aegirine-augite and albite (Figure 4a,b). In the BSE images, Pcl-I consistently exhibits well-developed oscillatory zoning (OZ) characterized by a series of straight, clear bands with alternating light and dark patterns parallel to the boundary of the crystal faces (Figure 4b).

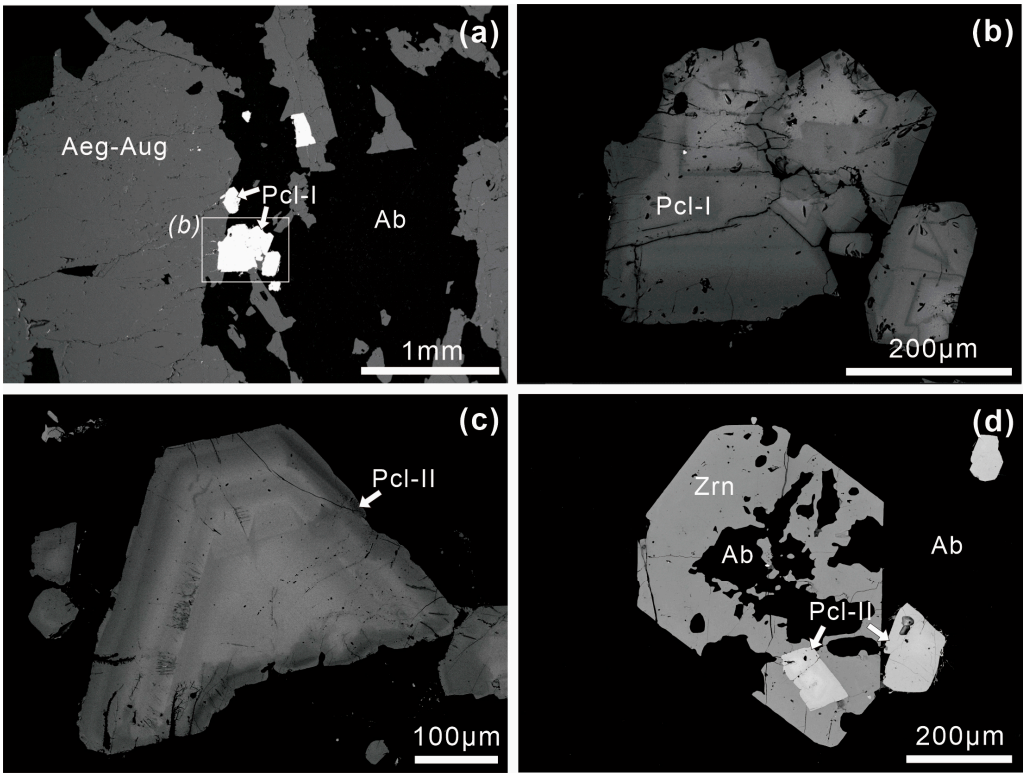


Figure 4. BSE images of pyrochlore in the Miyi pegmatite. (**a**,**b**) Pcl-I in Zone I contains OZ; (**c**) Pcl-II in Zone II is characterized by euhedral crystal and well-developed OZ; (**d**) Pcl-II is included in the magmatic zircon. Abbreviations: Ab, albite; Aeg-Aug, aegirine-augite; Pcl, pyrochlore; Zrn, zircon.

Pyrochlore supergroup minerals are more common in Zone II and exhibit a more complex internal texture compared to Zone I. Three types of pyrochlore supergroup minerals can be distinguished based on their zoning texture in the BSE images. Type II pyrochlore supergroup minerals (Pcl-II), characterized by their euhedral shape and well-developed OZ, are the most common type in Zone II (Figure 4c). Cracks can also occur inside the Pcl-II crystals (Figures 4c and 5b). The grain sizes of Pcl-II are 50–500 μm across (Figures 4c and 5a). Pcl-II is generally present as interstitial phases between rock-forming minerals such as albite and aegirine-augite (Figure 5a). However, a few Pcl-II crystals are also observed as inclusions within zircons (Figure 4d). Additionally, Pcl-II associated with albite is usually surrounded by anhedral pyrite (Figure 5a,b). Pcl-III grains are euhedral to subhedral and appear homogeneous in BSE images (Figure 5c). They are 20–200 μm across and inserted into the rock-forming minerals, with albites sometimes filling the cracks in Pcl-III

(Figure 5c). Pcl-IV is inhomogeneous with irregular zoning and sinuous bands in BSE images (Figure 5d). Pcl-IV grains are 20–50 μm across and closely associated with albite (Figure 5d). Tiny albite and pyrite may be included in Pcl-IV (Figure 5d).

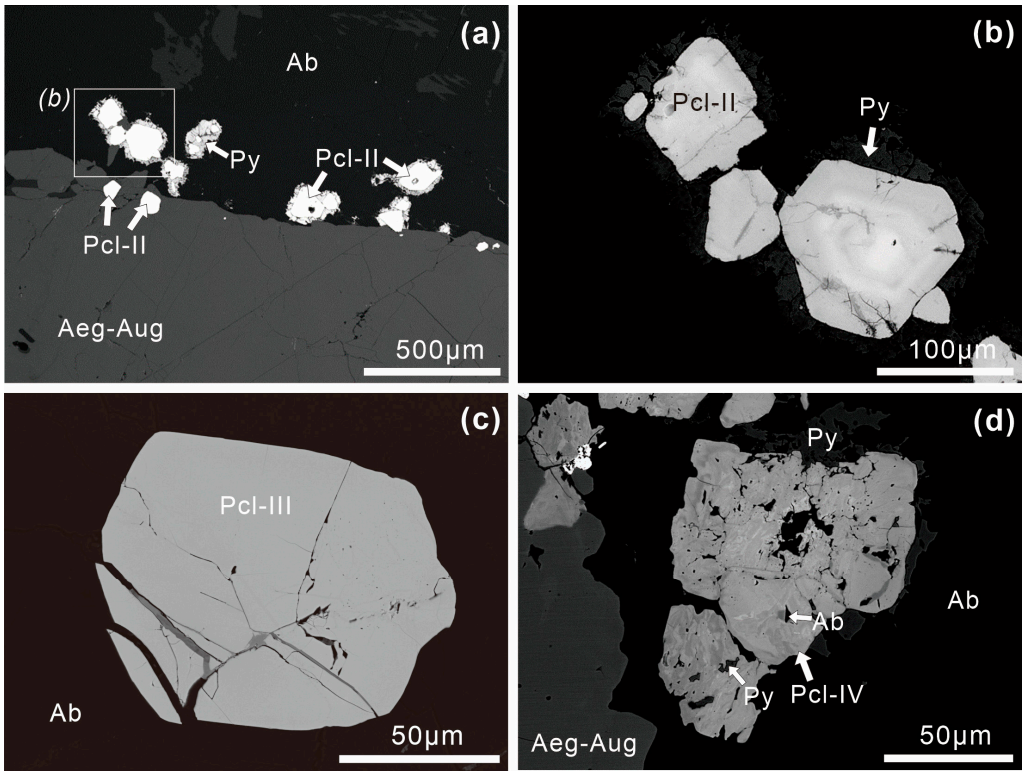


Figure 5. BSE images of pyrochlore in the Miyi pegmatite. (**a**,**b**) Pcl-II, associated with albite, is surrounded by anhedral pyrite; (**c**) Pcl-III in Zone II is homogeneous in BSE images; (**d**) Pcl-IV in Zone II shows irregular zoning and sinuous bands. Abbreviations: Ab, albite; Aeg-Aug, aegirine-augite; Pcl, pyrochlore; Py, pyrite.

4.2. Chemical Composition of Pyrochlore Supergroup Minerals

Based on the cations occupying the B-site, the composition of pyrochlore supergroup minerals in the Miyi pegmatite are concentrated in the Nb-rich member area, which is classified as pyrochlore (Figure 6a). In the A-site, the pyrochlores in the Miyi pegmatite are located close to the middle of the Na-Ca series, with fewer vacancies occupied (Figure 6b), leading to their further classification as hydroxycalciopyrochlore to fluorcalciopyrochlore (Figure 7).

In Zone I, Pcl-I has the highest TiO_2 (12.02–14.11 wt%) and UO_2 (13.92–17.40 wt%) contents but the lowest Na_2O (3.38–3.81 wt%), F (1.42–1.72 wt%), Nb_2O_5 (38.77–43.16 wt%), and Ce_2O_3 (2.79–3.08 wt%) contents among the four types of pyrochlores in the Miyi pegmatite (Figure 8; Table 1). Pcl-I also has relatively high contents of CaO (14.39–14.87 wt%) and Ta_2O_5 (3.31–4.06 wt%) (Figure 8; Table 1). In Zone II, Na_2O contents in Pcl-II (3.37–5.80 wt%) and Pcl-III (4.23–5.02 wt%) are comparable, but they abruptly increase in Pcl-IV (4.85–6.58 wt%) (Figure 8; Table 1). The F content increases gradually from Pcl-II (1.37–3.72 wt%) to Pcl-III (2.97–3.59 wt%) but shows less variation between Pcl-III and Pcl-IV (2.99–3.96 wt%) (Figure 8, Table 1). The Nb_2O_5 content increases gradually from Pcl-II (37.68–53.99 wt%) to Pcl-III (52.09–54.55 wt%) and increases with a compositional gap in Pcl-IV (51.13–62.43 wt%) (Figure 8; Table 1). The TiO_2 content varies contrarily from Pcl-II (9.00–15.13 wt%) through Pcl-III (9.01–9.55 wt%) to Pcl-IV (4.58–9.90 wt%) compared to the Nb_2O_5 content (Figure 8; Table 1). The Ce_2O_3 content decreases gradually from Pcl-II (3.21–5.47 wt%) through Pcl-III (3.46–4.08 wt%) to Pcl-IV (2.22–4.91 wt%) (Figure 8; Table 1). The UO_2 content also decreases from Pcl-II (bdl—18.45 wt%) to Pcl-III (bdl—2.55 wt%)

but shows less variability in Pcl-IV (bdl—2.32 wt%) (Figure 8; Table 1). The CaO content increases from Pcl-II (10.40–15.90 wt%) to Pcl-III (16.27–17.15 wt%) but then decreases in Pcl-IV (14.17–16.02 wt%). By contrast, the Ta_2O_5 content varies contrarily from Pcl-II (1.24–4.64 wt%) through Pcl-III (1.54–3.07 wt%) to Pcl-IV (0.99–3.87 wt%) (Figure 8; Table 1).

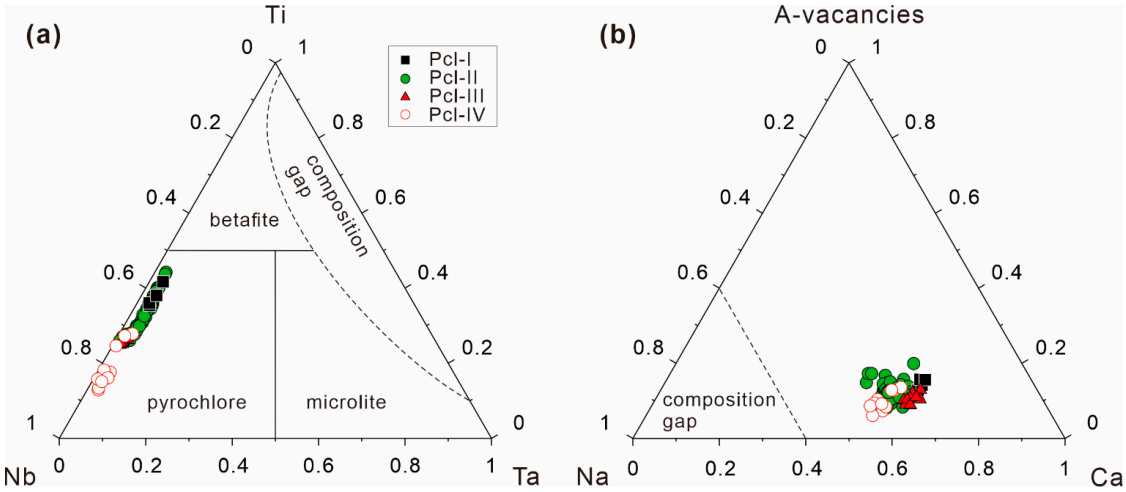


Figure 6. (**a**) Ternary classification scheme based on cations in the B-site, including Nb, Ti, and Ta (modified by [22]), and (**b**) ternary diagram of vacancies and cations in the A-site, including Ca and Na for pyrochlore supergroup minerals in the Miyi pegmatite. The compositional gap zones represented by a dotted line at the A-site were proposed by [22] using 1030 analysis data.

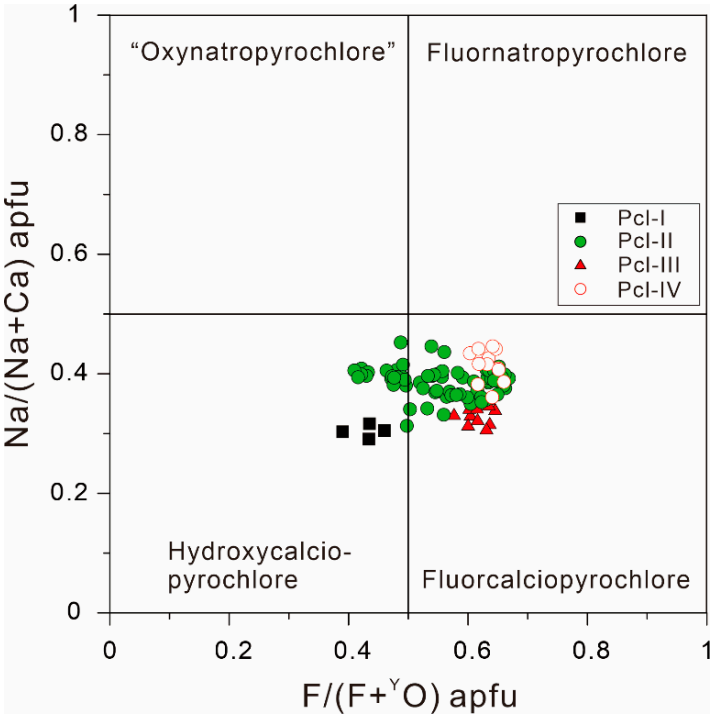


Figure 7. Compositional diagram of atomic proportions in both the A- and Y-sites of pyrochlores in the Miyi pegmatite.

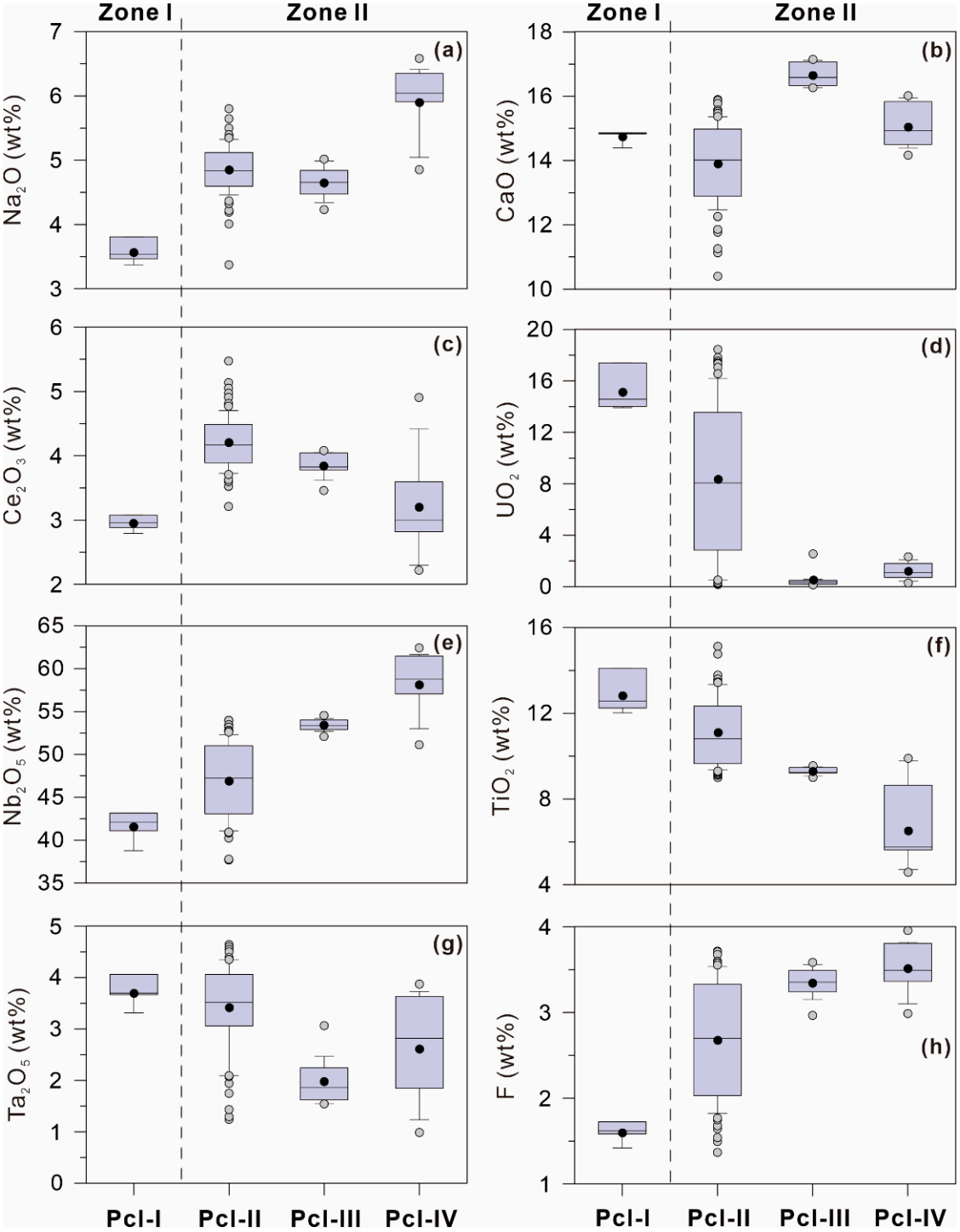


Figure 8. Percentile box-and-whisker plots showing the representative major or minor element ((**a**) Na_2O, (**b**) CaO, (**c**) Ce_2O_3, and (**d**) UO_2 in A-site; (**e**) Nb_2O_5, (**f**) TiO_2, and (**g**) Ta_2O_5 in B-site; and (**h**) F in Y-site) contents in four types of pyrochlores in the Miyi pegmatite. The boxes mark the 25th and 75th percentiles, and the lines within the boxes indicate the median values. The whiskers extend from the 10th to 90th percentiles. The gray circles beyond the whiskers and the dark circles are individual extreme values and the mean values, respectively.

Table 1. EPMA compositions of pyrochlores in different texture zones in the Miyi pegmatite.

	Zone I			Zone II								
	Pcl-I			Pcl-II			Pcl-III			Pcl-IV		
EPMA (wt%)	**mean (*n* = 4)**	**max**	**min**	**mean (*n* = 71)**	**max**	**min**	**mean (*n* = 12)**	**max**	**min**	**mean (*n* = 12)**	**max**	**min**
Na_2O	3.56 (0.19)	3.81	3.38	4.85 (0.40)	5.80	3.37	4.65 (0.26)	5.02	4.23	5.90 (0.57)	6.58	4.85
CaO	14.74 (0.23)	14.87	14.39	13.89 (1.26)	15.90	10.40	16.65 (0.35)	17.15	16.27	15.04 (0.65)	16.02	14.17
PbO	0.73 (0.06)	0.82	0.69	0.51 (0.18)	0.84	0.21	0.31 (0.06)	0.37	bdl	0.31 (0.05)	0.37	bdl
BaO	bdl	bdl	bdl	bdl	bdl	bdl	bdl)	bdl	bdl	bdl	bdl	bdl
UO_2	15.12 (1.62)	17.40	13.92	8.34 (5.78)	18.45	bdl	0.51 (0.66)	2.55	bdl	1.19 (0.66)	2.32	bdl
ThO_2	1.05 (0.15)	1.18	0.83	1.87 (1.05)	4.60	0.59	4.12 (0.65)	5.18	2.56	2.51 (1.40)	5.04	0.64
Y_2O_3	0.19 (0.06)	0.27	bdl	0.27 (0.08)	0.54	0.16	0.20 (0.05)	0.27	bdl	0.22 (0.22)	0.67	bdl
La_2O_3	0.36 (0.13)	0.48	0.24	0.81 (0.20)	1.15	0.39	0.85 (0.13)	1.09	0.64	0.71 (0.23)	1.15	0.45
Ce_2O_3	2.95 (0.13)	3.08	2.79	4.20 (0.42)	5.47	3.21	3.84 (0.19)	4.08	3.46	3.20 (0.80)	4.91	2.22
Pr_2O_3	0.27 (0.24)	0.51	bdl	0.56 (0.20)	1.16	bdl	0.39 (0.21)	0.82	bdl	0.39 (0.14)	0.72	0.23
Nd_2O_3	0.85 (0.07)	0.90	0.75	1.20 (0.31)	1.87	0.57	0.73 (0.10)	0.86	0.51	0.56 (0.19)	0.84	0.25
Sm_2O_3	0.21 (0.07)	0.31	bdl	bdl	0.33	bdl	bdl	bdl	bdl	bdl	bdl	bdl
TiO_2	12.82 (0.94)	14.11	12.02	11.10 (1.56)	15.13	9.00	9.29 (0.18)	9.55	9.01	6.51 (1.86)	9.90	4.58
ZrO_2	bdl	bdl	bdl	0.21 (0.11)	0.68	bdl	bdl	0.19	bdl	bdl	bdl	bdl
Nb_2O_5	41.54 (2.08)	43.16	38.77	46.88 (4.38)	53.99	37.68	53.42 (0.72)	54.55	52.09	58.11 (3.58)	62.43	51.13
Ta_2O_5	3.69 (0.31)	4.06	3.31	3.41 (0.86)	4.64	1.24	1.98 (0.45)	3.07	1.54	2.61 (1.03)	3.87	0.99
MnO	0.06 (0.04)	0.09	bdl	0.11 (0.07)	0.30	bdl	bdl	0.14	bdl	0.09 (0.05)	0.17	bdl
FeO	0.34 (0.11)	0.51	0.28	0.14 (0.09)	0.55	bdl	0.12 (0.10)	0.31	bdl	0.19 (0.10)	0.39	0.09
F	1.60 (0.13)	1.72	1.42	2.68 (0.66)	3.72	1.37	3.34 (0.18)	3.59	2.97	3.51 (0.30)	3.96	2.99
Total	99.56 (0.36)	99.96	99.25	100.08 (1.81)	102.50	93.47	99.32 (0.50)	100.15	98.39	99.69 (0.74)	100.79	98.31
based on ΣB = 2												
Na	0.43 (0.02)	0.46	0.41	0.57 (0.04)	0.67	0.41	0.54 (0.03)	0.58	0.48	0.69 (0.07)	0.77	0.55
Ca	0.98 (0.01)	0.99	0.96	0.91 (0.07)	1.02	0.73	1.06 (0.02)	1.09	1.03	0.97 (0.04)	1.03	0.92
Pb	0.01	0.01	0.01	0.01	0.01	bdl	0.01	0.01	bdl	0.01	0.01	bdl
Ba	bdl	bdl	bdl	bdl	bdl	bdl	bdl	bdl	bdl	bdl	bdl	bdl
U	0.21 (0.02)	0.24	0.19	0.11 (0.08)	0.25	bdl	0.01 (0.01)	0.03	bdl	0.02 (0.01)	0.03	bdl
Th	0.02	0.02	0.01	0.03 (0.01)	0.06	0.01	0.06 (0.01)	0.07	0.04	0.03 (0.02)	0.07	0.01
Y	0.01	0.01	bdl	0.01	0.02	0.01	0.01	0.01	bdl	0.01 (0.01)	0.02	bdl
La	0.01	0.01	0.01	0.02	0.03	0.01	0.02	0.02	0.01	0.02 (0.01)	0.03	0.01
Ce	0.07	0.07	0.06	0.09 (0.01)	0.12	0.07	0.08	0.09	0.08	0.07 (0.02)	0.11	0.05
Pr	0.01 (0.01)	0.01	bdl	0.01 (0.01)	0.03	bdl	0.01 (0.01)	0.02	bdl	0.01	0.02	0.01
Nd	0.02	0.02	0.02	0.03 (0.01)	0.04	0.01	0.02	0.02	0.01	0.01	0.02	0.01
Sm	bdl	0.01	bdl	bdl	0.01	bdl	bdl	bdl	bdl	bdl	bdl	bdl
ΣA	1.76 (0.02)	1.79	1.74	1.79 (0.03)	1.86	1.67	1.80 (0.02)	1.83	1.76	1.83 (0.04)	1.89	1.76
Ti	0.75 (0.06)	0.83	0.70	0.64 (0.10)	0.88	0.51	0.52 (0.01)	0.53	0.51	0.37 (0.10)	0.55	0.26
Zr	bdl	bdl	bdl	0.01	0.02	bdl	bdl	0.01	bdl	bdl	bdl	bdl
Nb	1.166 (0.06)	1.21	1.09	1.29 (0.10)	1.45	1.05	1.44 (0.02)	1.46	1.41	1.58 (0.10)	1.68	1.37
Ta	0.06 (0.01)	0.07	0.06	0.06 (0.01)	0.08	0.02	0.03 (0.01)	0.05	0.03	0.04 (0.02)	0.06	0.02
Mn	bdl	0.01	bdl	0.01	0.02	bdl	bdl	0.01	bdl	0.01	0.01	bdl
Fe	0.02 (0.01)	0.03	0.02	0.01 (0.01)	0.03	bdl	0.01 (0.01)	0.02	bdl	0.01 (0.01)	0.02	0.01
ΣB	2.00	2.00	2.00	2.00	2.00	2.00	2.00	2.00	2.00	2.00	2.00	2.00
F	0.31 (0.03)	0.34	0.28	0.51 (0.12)	0.71	0.27	0.63 (0.03)	0.67	0.56	0.67 (0.06)	0.74	0.56
O	6.42 (0.03)	6.44	6.38	6.39 (0.04)	6.46	6.32	6.39 (0.02)	6.41	6.35	6.38 (0.04)	6.44	6.32

Notes: Numbers in parentheses are standard deviations. bdl = below detection limit.

4.3. Compositional Zoning of Pyrochlore Supergroup Minerals

The BSE images of the OZ in Pcl-I and Pcl-II always exhibit relatively darker rims compared to the core (Figures 4c and 5b). The X-ray elemental map of Pcl-II reveals that the brightness of the BSE images is consistent with the compositional variations in Ti, U, Ca, and Nb, and roughly fits the variable Na and F contents. The bright bands are enriched in Ti and U, while the dark ones are enriched in Nb, Na, F, and Ca (Figure 9). Meanwhile, the Ce and Ta compositional variation is independent of the OZ brightness and has less core-to-rim variation (Figure 9). The compositional profiles of Pcl-II further reveal that the contents of CaO, F, Nb_2O_5, Ce_2O_3, and Na_2O increased, while the contents of TiO_2 and UO_2 decreased from the core to the rim (Figure 10).

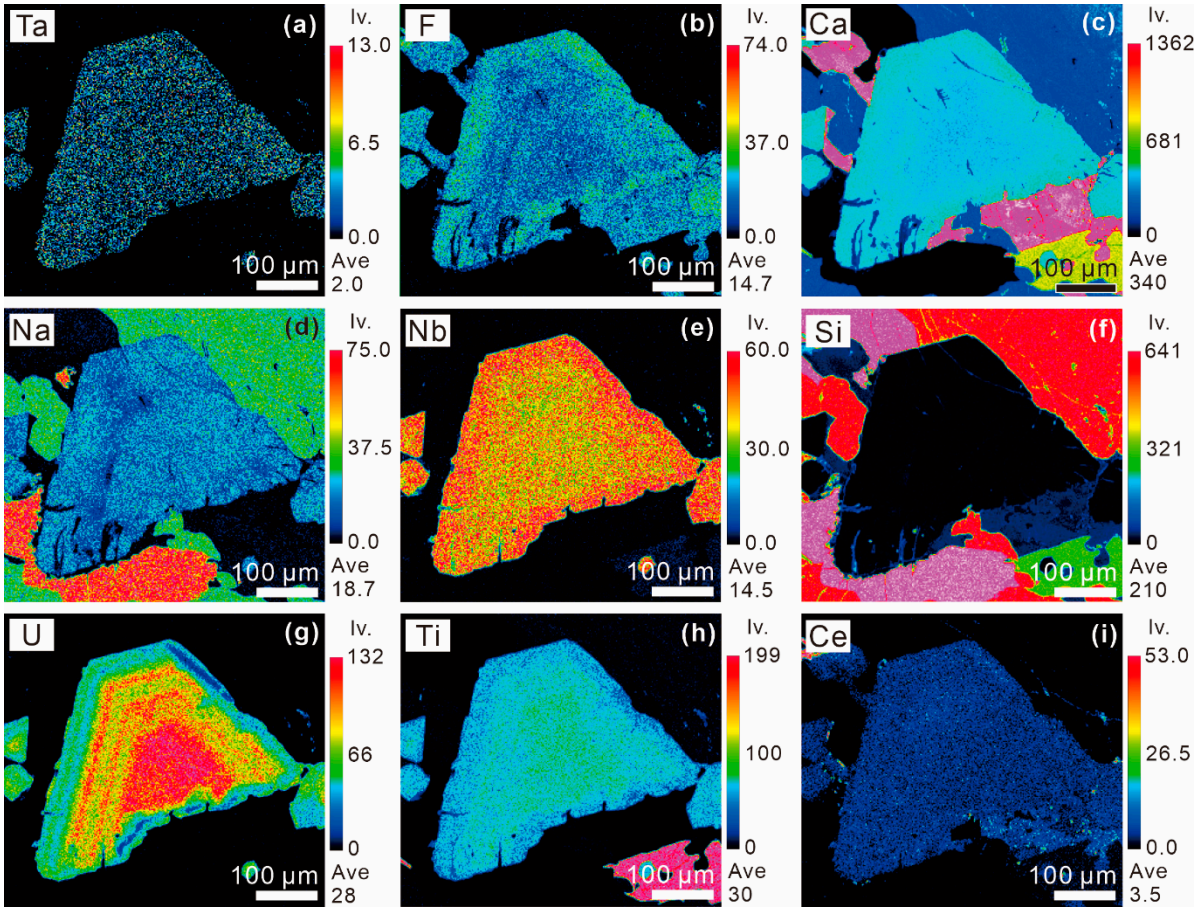


Figure 9. X-ray compositional maps of (**a**–**i**) Ta, F, Ca, Na, Nb, Si, U, Ti, and Ce, respectively, in the Pcl-II shown in Figure 4c in Zone II of the Miyi pegmatite.

X-ray elemental map of Pcl-IV reveals that the bright region exhibits distinctly higher Ti and Ce contents but lower F and Na contents than the dark region (Figure 11). The U content is concentrated in the brightest veins in Pcl-IV (Figure 11). The quantitative data further reveal that the contents of TiO_2, UO_2, and Ce_2O_3 decreased from the bright region (TiO_2 = 5.29–9.90 wt%, UO_2 = 0.43–2.32 wt%, Ce_2O_3 = 2.65–4.91 wt%) to the dark region (TiO_2 = 4.58–5.80 wt%, UO_2 = 0.29–1.81 wt%, Ce_2O_3 = 2.22–3.43 wt%). However, the contents of Na_2O, F, and Nb_2O_5 increased from the bright region (Na_2O = 4.85–6.02 wt%, F = 2.99–3.40 wt%, Nb_2O_5 = 51.13–60.10 wt%) to the dark region (Na_2O = 6.06–6.58 wt%, F = 3.58–3.96 wt%, Nb_2O_5 = 58.74–62.43 wt%) (Table 1).

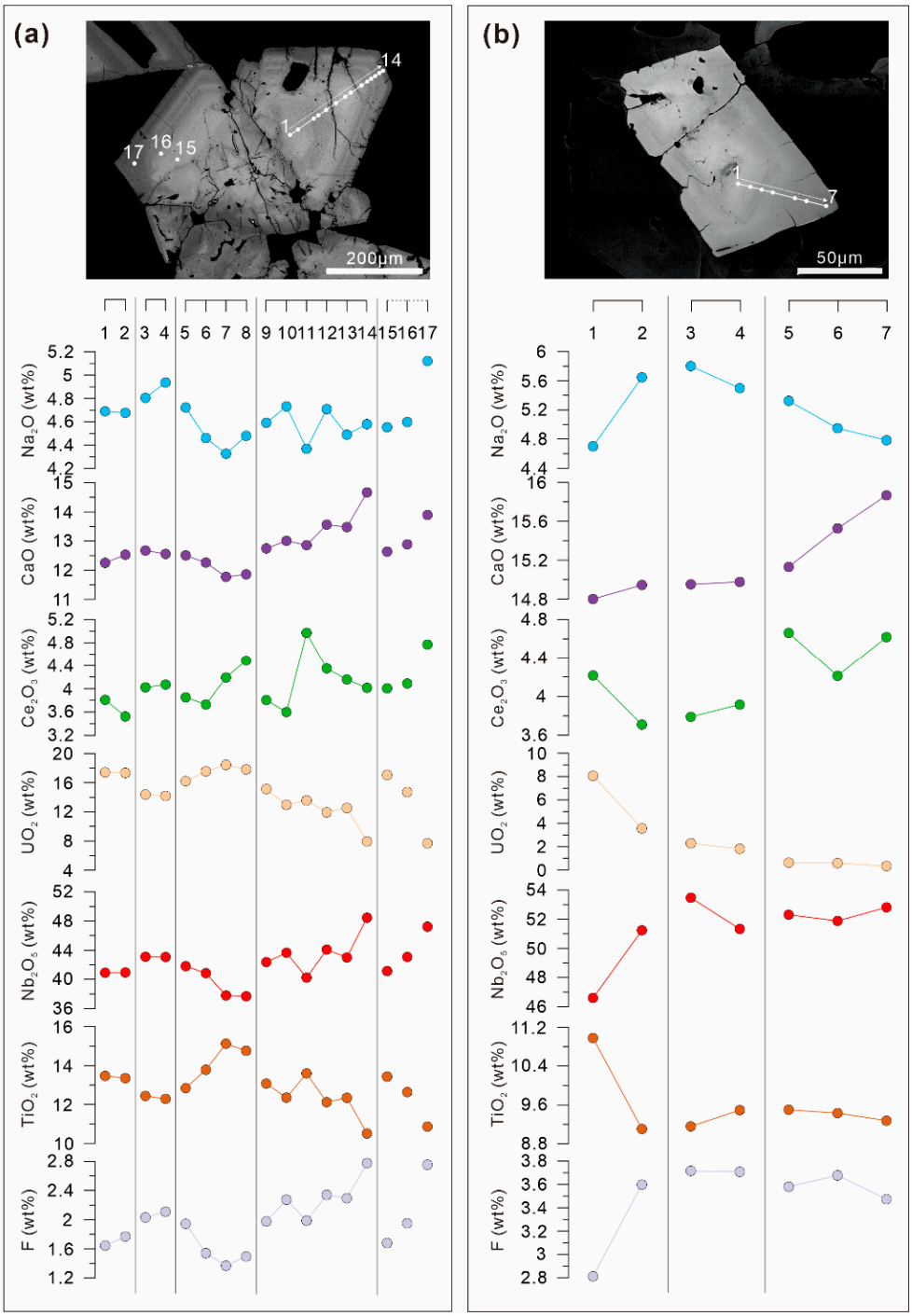


Figure 10. Chemical profiles display the oscillatory compositional variations in Pcl-II in Zone II of the Miyi pegmatite. (**a**) Pcl-II associated with albite and aegirine-augite, and (**b**) Pcl-II included in zircon as shown in Figure 4d. The numbers and white dots indicate analysis points.

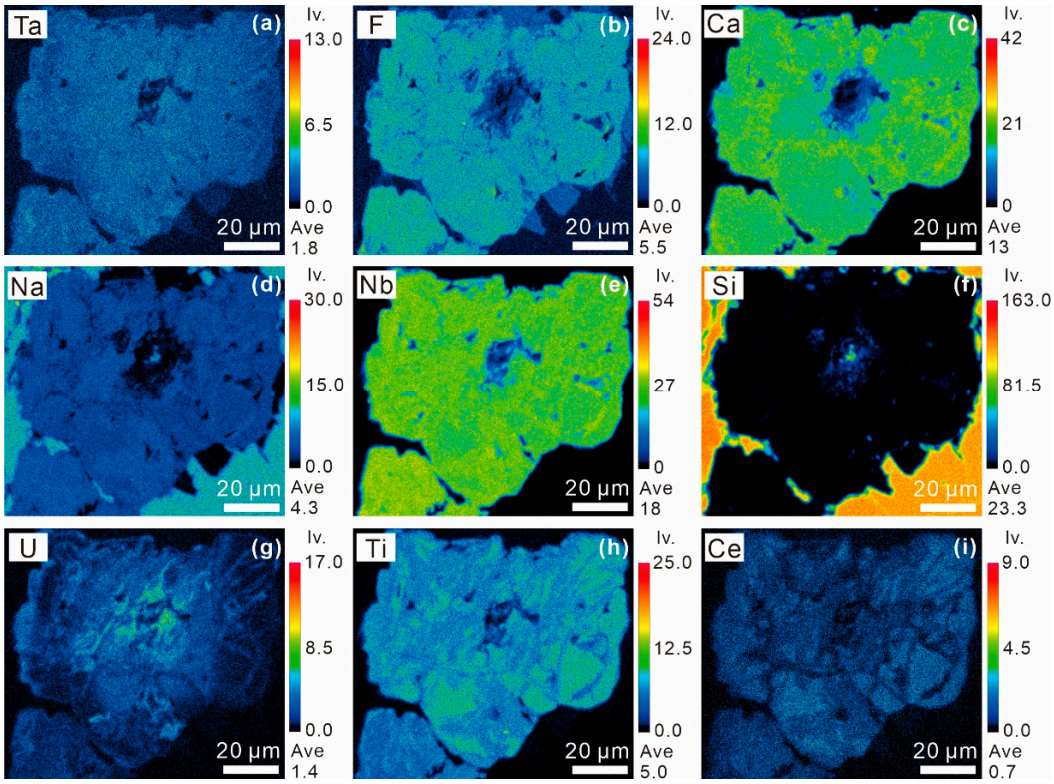


Figure 11. X-ray compositional maps of (**a**–**i**) Ta, F, Ca, Na, Nb, Si, U, Ti, and Ce, respectively, in the Pcl-IV shown in Figure 5d in Zone II of the Miyi pegmatite.

5. Discussion

5.1. Substitution of Elements in the Pyrochlore in the Miyi Pegmatite

The chemical variations of pyrochlore in the Miyi pegmatite can be used as a proxy for alkalic magmatic evolution-controlled Nb mineralization since it can contain Nb, Na, F, Ca, and Ti. Both the crystal chemical and geochemical mechanisms contribute to variations in the concentrations of these elements in pyrochlore. In the Miyi pegmatite, the cations exhibit large compositional variations both in the A-site (including Na, Ca, U, and REE) and the B-site (including Ti, Na, and Ta). Additionally, anions, including F and OH^-, are substituted with the pyrochlore compositions varying along the series of hydroxycalciopyrochlore and fluorcalciopyrochlore (Figure 7). As shown in Figure 8, Pcl-II, with well-developed OZ, exhibits the largest variation in the elements; conversely, the homogeneous pyrochlore crystals (Pcl-III) exhibit minimal chemical variations (Figure 8).

Since the cations occupying the A-site or B-site are polyvalent in pyrochlore, a combination of substitutions could occur [45]. The most common scenario is the substitution occurring in both the A- and B-site [46]. The end-member $Ca_2TiNbO_6(OH,F)$ can be generated by a coupled substitution involving the cations in both A and B sites, where REE is constant, according to:

$$Ca^{2+} + Ti^{4+} = Na^{+} + Nb^{5+} \quad (1)$$

When Ca is constant, the end-member $Ca(REE)Ti_2O_6(OH,F)$ can be generated by a coupled substitution according to:

$$REE^{3+} + 2Ti^{4+} = Na^{+} + 2Nb^{5+} \quad (2)$$

When Na is constant, the end-member $Na(REE)TiNbO_6(OH,F)$ can be generated by:

$$REE^{3+} + Ti^{4+} = Ca^{2+} + Nb^{5+} \quad (3)$$

When the coupled cation substitution involves only the A-site, with constant Nb and Ti, REE can be incorporated and the end-member $REE_{0.5}Na_{0.5}CaNb_2O_6(OH,F)$ can be generated by:

$$Na^{+} + REE^{3+} = 2Ca^{2+} \quad (4)$$

Different from the heterovalent isomorphism in the previous schemes, the substitution of U and Ti is homovalent, with the following equations:

$$U^{4+} + 3Ti^{4+} = Na^{+} + 3Nb^{5+} \quad (5)$$

$$U^{4+} + 2Ti^{4+} = Ca^{2+} + 2Nb^{5+} \quad (6)$$

Based on the linear negative correlations of the plots of elemental pairs shown in Figure 12, the selective enrichment of elements in the pyrochlore in the Miyi pegmatite is controlled by the chemical substitution and valence state of the elements as shown above.

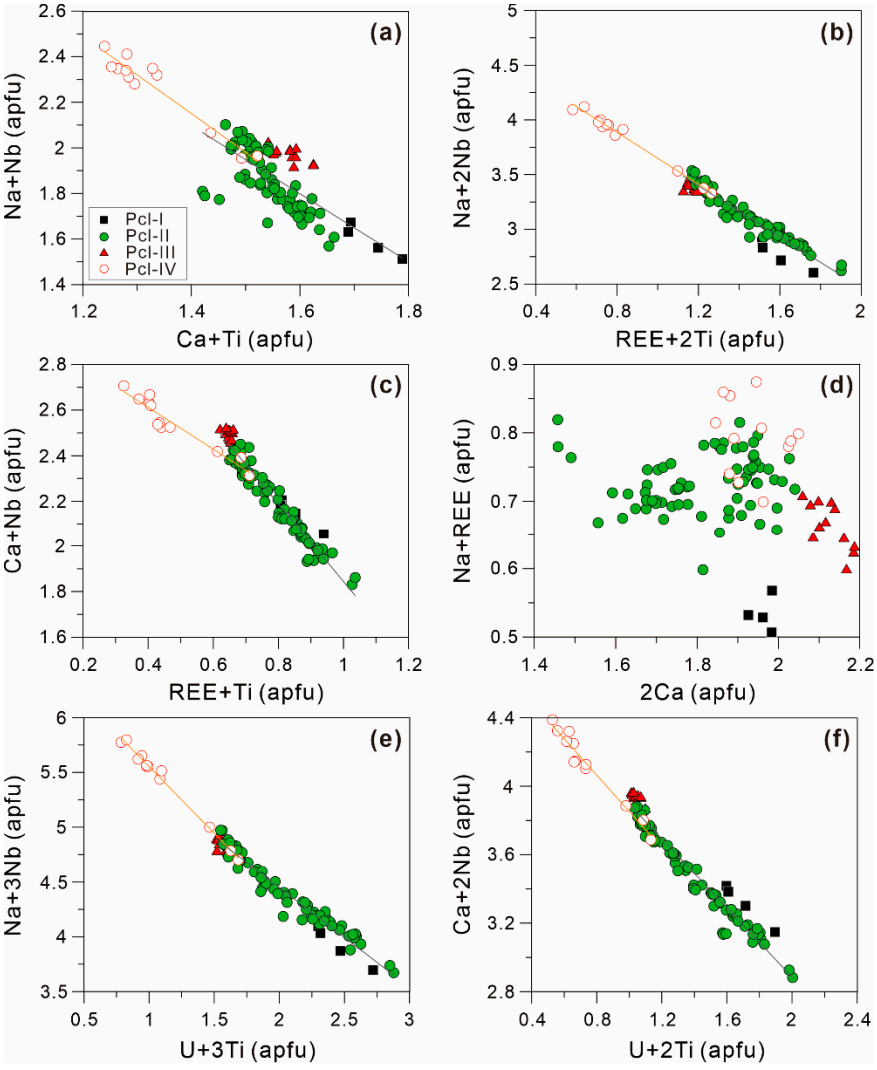


Figure 12. Plots of (**a**) Ca + Ti vs. Na + Nb, (**b**) REE + 2Ti vs. Na + 2Nb, (**c**) REE + Ti vs. Ca + Nb, (**d**) 2Ca vs. Na + REE, (**e**) U + 3Ti vs. Na + 3Nb, and (**f**) U + 2Ti vs. Ca + 2Nb of four types of pyrochlore in the Miyi pegmatite.

The decorrelation in the compositional plots of Ca vs. Na + REE in the pyrochlore indicates that cation substitution cannot merely involve the A-site (Figure 12d). Notably, the pyrochlore with OZ, especially the Pyl-II, presents a good linear permutation relationship, illustrating that the zoning texture and the distribution of component bands can be

controlled by crystal chemistry (Figure 12). The linear slope of the substitution equation in Pyl-IV is slightly different from the other types of pyrochlore, illustrating the different compositions of melt for their crystallization (Figure 12a,c,e).

5.2. Genesis of Four Types of Pyrochlores in the Miyi Pegmatite

In carbonatites and syenites, pyrochlore crystallizes mainly directly in the magma, leading to metallogenic mechanisms related to Nb mineralization focusing on magmatic evolution e.g., [27]. However, the alteration of pyrochlore also indicates the significant role of hydrothermal fluids on Nb mineralization e.g., [25,26,28,47–51]. For instance, the pyrochlore in the St Honoré carbonatite in Canada exhibited irregular patchy zoning and overgrowth representing species that crystallized from a carbonatitic magma that had undergone fluid exsolution [47]. In syenite from south Greenland, fluid alteration caused the primary pyrochlore with weak OZ to be overprinted by alteration textures resembling a mosaic or tortoiseshell pattern in BSE images or cut by vein-like areas of alteration [26]. Pyrochlore can be decomposed to a stronger degree through structural destruction, resulting in in situ crystallization of secondary ferrocolumbite, uraninite, Nb-bearing rutile, and fergusonite-(Y) [29,30]. This process is also characterized by the local exchange and re-equilibration of fluid-mobile elements, which can reconstruct the metallogenic mechanism of Nb and the properties of fluids in the magmatic-hydrothermal transition stage [28,47]. In the Pan-Xi area, the enrichment of lighter whole-rock B isotopes in the Nb-mineralized syenitic dikes than in the Nb-poor dikes indicates that hydrothermal fluids are a critical factor for Nb mineralization [12]. Meanwhile, the chemical and petrographic characteristics of zircons in the Miyi pegmatite illustrate that both magmatic and hydrothermal processes facilitate Nb and REE mineralization [13].

In pyrochlore, the chemical composition varies systematically from core to rim, often displaying one or more superimposed, sharply defined, parallel crystal faces, and appearing most commonly near the outer part of the crystal, characterizing it as primary zonation that crystallized directly in the magma [25]. Both Pcl-I and Pcl-II in Miyi pegmatite containing OZ are magmatic in origin because they exhibit such characteristics (Figure 4). Pcl-I and Pcl-II were considered to crystallize before the fluids became saturated in the magma, as Pcl-I crystallized in Zone I, in which the magma is less evolved, viscous, and anhydrous [13]. Some euhedral Pcl-II crystallized in the magmatic zircon, indicating that Pcl-II crystallized earlier or simultaneously during zircon crystallization in the magma (Figure 4d). Under these conditions, zoning can develop in self-crystallized pyrochlore in a comparatively stable environment until the fractional crystallization of the magma is completed. This is a result of equilibrium fractional crystallization during normal geochemical evolution [52], as the Pcl-II exhibits largely and successively compositional variations (Figure 13). The origin of OZ in Nb-Ta oxide minerals can be controlled, on one hand, by the dynamic growth conditions of periodic variations in crystallization and diffusion velocity at the melt-crystal interface [53], and on the other hand, by the fluctuating P-T-X conditions in the melt [54]. In the Miyi pegmatite, the OZ structure in pyrochlore was formed through disequilibrium crystallization in an oscillatory environment in which the variation in Nb, Ca, and Na is complemented by the compositions of U and Ti based on the lattice substitution of the elements mentioned above.

In Zone II of the Miyi pegmatite, Pcl-III can also be considered magmatic in origin, as its chemical evolution is coherent and consistent with the Pcl-II trend (Figure 12). Unlike the OZ texture in Pcl-II, the homogeneous and less variable composition of Pcl-III illustrates a more stable P-T-X crystallization condition in the melt. It may have crystallized in the most evolved magma because Pcl-III exhibits comparable Nb, F, and Ca contents with the highest values in Pcl-II (Figures 8 and 13). The high amounts of compositional pyrochlore data show a compositional gap in the Na end member in the Na-Ca series [22]. This is because the theoretical nonexistence of "oxynatropyrochlore" as its end member $Na_2Nb_2O_7$ cannot reach electrovalence equilibrium [22]. Therefore, the Na content in Pcl-III will not increase as Na in the melt, as Na in the crystal lattices of pyrochlore is not a superior occupying ion.

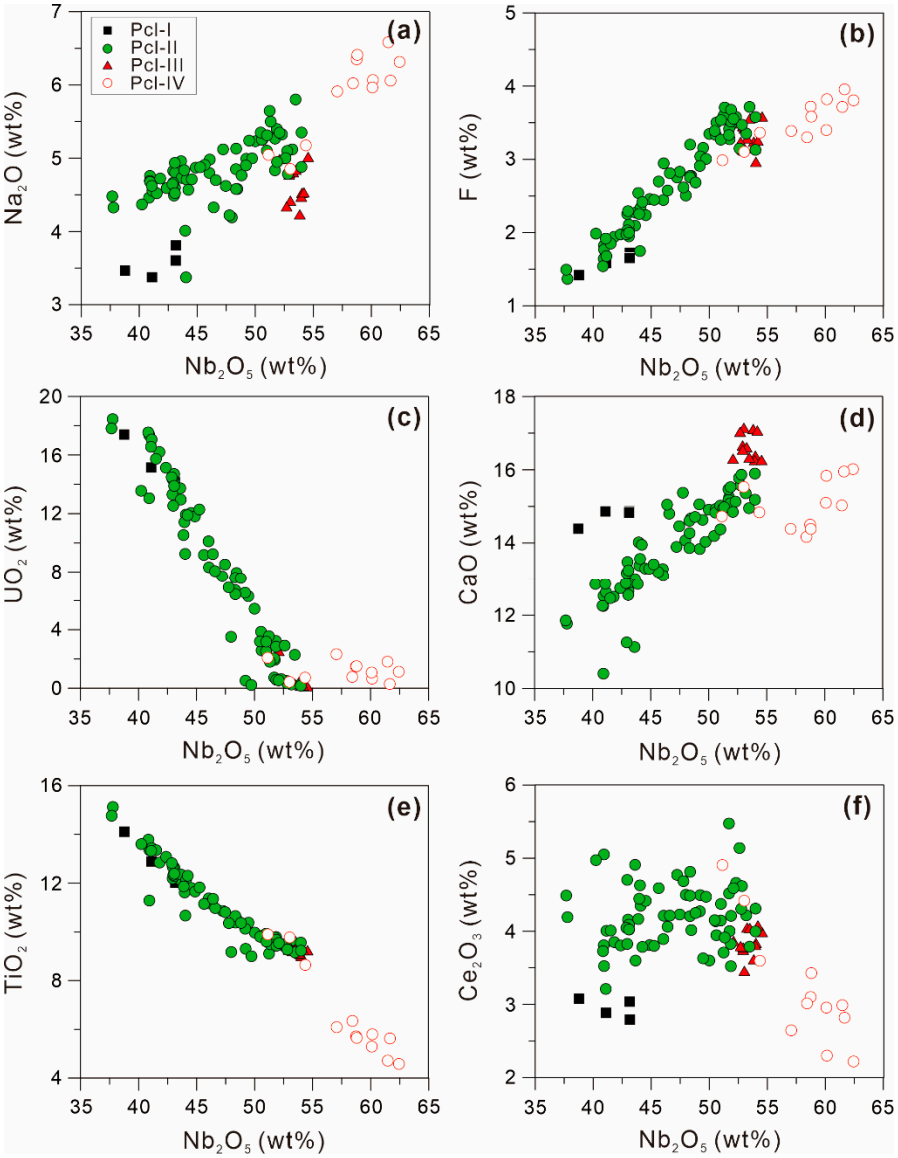


Figure 13. Plots of (**a**) Nb_2O_5 vs. Na_2O, (**b**) Nb_2O_5 vs. F, (**c**) Nb_2O_5 vs. UO_2, (**d**) Nb_2O_5 vs. CaO, (**e**) Nb_2O_5 vs. TiO_2, and (**f**) Nb_2O_5 vs. Ce_2O_3 of four types of pyrochlores in the Miyi pegmatite.

Pcl-IV is considered to have a hydrothermal origin based on its irregular zoning texture. Different from the straight and regular OZ, Norton and Dutrow [55] proposed that a complex dynamic system is involved in magmatic-hydrothermal processes where the existence of a supercritical fluid can transform the system into a disordered state. This system provides a complex and variable environment for crystallization conducive to the growth of complex and multi-stage zonation. The significant and discontinuous increase in Na_2O from Pcl-III to Pcl-IV, which is a trend opposite to that observed from Pcl-II to Pcl-III, suggests that Pcl-IV cannot crystallize in a higher evolved magma (Figures 8a and 13a). The hydrothermal crystallization environment also results in Pcl-IV presenting a different compositional variation trend compared with the magmatic pyrochlores based on the changes in the linear slope of the substitution equation and the compositional gap in Nb_2O_5 in Pcl-IV (Figure 12a,c,e).

5.3. Nb Mineralization during the Magmatic-Hydrothermal Evolution in the Miyi Pegmatite

The NFY pegmatite occurs mainly in intraplate tectonic environments and is typically associated with rifting, faulting, and/or crustal extension. In such settings, magma with oceanic island basalt (OIB) characteristics can be generated, leading to a very high Nb

content [2]. In the Miyi pegmatite, the crystal chemistry of pyrochlore reconstructs the significant role of both the late-stage magmatic evolution and hydrothermal alteration in the two mineralization periods.

The first period of Nb mineralization produces primary magmatic pyrochlore assemblages (Figures 4 and 5a–c), which are formed through the crystallization of fractionated peralkaline magma rich in rare metals. In magmatic pyrochlore, the decrease in TiO_2 contents from Pcl-I to Pcl-III is mainly caused by the crystallization of ilmenite and biotite in the magma (Figure 13e) [56]. The synchronous decrease in UO_2 content may be controlled by the crystallization of monazite, which is usually the earliest crystallized REE mineral due to its very low solubility [57], and zircon (Figure 13c). The Na content in the melt increases with magmatic evolution, as evidenced by increasing Na content in zircons and pyrochlore from Zone I to Zone II [13]. The solubility of Nb in the alkaline magma can significantly increase by combining with more non-bridging oxygens (NBOs) generated by the excess Na in the melt [16,17,19,58]. Therefore, the synchronous increase in Na and Nb from Pcl-I to Pcl-III and from the core to the rim in Pcl-II illustrates that Na facilitates the enrichment of Nb in the Miyi pegmatite (Figures 10 and 13a). In the alkaline melt, high F content is considered to have a positive role in prolonging the fractional crystallization and the crystallization of albite by reducing the viscosity and liquidus temperature of the magma [59–61], as evidenced by the synchronous increase in F, Nb, and Na contents in the magmatic pyrochlore in the Miyi pegmatite (Figure 13).

During the subsequent crystallization of pyrochlore by hydrothermal fluids, Nb is remobilized and further enriched in Zone II of the Miyi pegmatite (Figure 8e). The decreased Ce_2O_3 content in the hydrothermal pyrochlore indicates that REE has been mineralized as monazite, allanite, britholite, etc., in the hydrothermal fluids (Figure 8c) [13]. The distinctly higher Na and F contents in the hydrothermal pyrochlore than in the magmatic ones indicate that Na and F, which are compatible with the hydrothermal fluids, have a more significant role on Nb mineralization (Figure 13a,b), which also aligns with the crystal chemistry of hydrothermal zircons in the Miyi pegmatite [13]. Indeed, solubility experiments have shown that the addition of Na^+ in aqueous solutions enhances the complexation of F^- and Nb^{5+}, which may improve the solubility of Nb in the fluid [62–64]. The later-formed pyrite around Pcl-II indicates that such Na-F-rich fluid solution is under reductive conditions (Figure 5a,b), with the same properties of fluid also occurring in the Baicao syenitic Nb deposit [30]. Although the hydrothermal fluid has a more effective effect on the further enrichment of Nb, the primary magmatic ore assemblages are still the dominant Nb mineralization.

6. Conclusions

The pyrochlore supergroup minerals present in the Miyi pegmatite in the Pan-Xi area are Nb-dominant, and their compositions are located near the middle of the Na-Ca series with fewer vacancies, further classified as hydroxycalciopyrochlore to fluorcalciopyrochlore. Four types of pyrochlores are present in the Miyi pegmatite and can be identified as magmatic or hydrothermal types. The magmatic pyrochlores are euhedral and exhibit well-developed oscillatory zoning textures, while the hydrothermal pyrochlores, displaying irregular zoning, crystallize under the influence of hydrothermal fluids that transform the magmatic system into a disordered state.

The crystal chemistry of the four types of pyrochlores consists of a two-stage Nb mineralization process in the Miyi pegmatite. The first mineralization stage produces primary magmatic pyrochlores resulting from the fractional crystallization of a fractionated peralkaline magma rich in rare metals. During the magmatic-hydrothermal transition stage, the enrichment of Na and F in the fluid facilitates transportation and has a more effective effect on further enrichment of Nb in pyrochlore.

Author Contributions: Conceptualization, R.Y. and X.S.; field investigation, S.W., X.S. and R.Y.; methodology, B.W.; data curation, B.W. and R.Y.; resources, X.S. and S.W.; writing–original draft preparation, R.Y.; writing–review and editing, R.Y. and X.S.; visualization, R.Y.; supervision, R.Y. and X.S.; funding acquisition, X.S., R.Y. and S.W. All authors have read and agreed to the published version of the manuscript.

Funding: This research was financially supported by the National Key Research and Development Program of China (Grant No. 2018YFA0702605) and the National Natural Science Foundation of China (NSFC Project 42172075, 42272106).

Data Availability Statement: Raw data are available from the corresponding author upon reasonable request.

Acknowledgments: We thank Qian Ren (East China University of Technology) for the chemical analysis. We thank Jian-Lin Liao (Sun Yat-sen University) for assistance with fieldwork and collecting samples. We are grateful to three anonymous reviewers for their careful reviews and constructive comments.

Conflicts of Interest: The authors declare no conflict of interest.

References

1. Linnen, R.L.; van Lichtervelde, M.; Černý, P. Granitic pegmatites as sources of strategic metals. *Elements* **2012**, *8*, 275–280. [CrossRef]
2. Williams-Jones, A.E.; Vasyukova, O.V. Niobium, Critical metal, and progeny of the mantle. *Econ. Geol.* **2023**, *118*, 837–855. [CrossRef]
3. Kogarko, L.N.; Lahaye, Y.; Brey, G.P. Plume-related mantle source of super-large rare metal deposits from the Lovozero and Khibina massifs on the Kola Peninsula, Eastern part of Baltic Shield: Sr, Nd and Hf isotope systematics. *Miner. Petrol.* **2010**, *98*, 197–208. [CrossRef]
4. Pirajno, F. Intracontinental anorogenic alkaline magmatism and carbonatites, associated mineral systems and the mantle plume connection. *Gondwana Res.* **2014**, *27*, 1181–1216. [CrossRef]
5. He, B.; Xu, Y.G.; Chung, S.L.; Xiao, L.; Wang, Y. Sedimentary evidence for a rapid, kilometer-scale crustal doming prior to the eruption of the Emeishan flood basalts. *Earth Planet. Sc. Lett.* **2003**, *213*, 391–405. [CrossRef]
6. Shellnutt, J.G.; Zhou, M.F. Permian peralkaline, peraluminous and metaluminous A-type granites in the Panxi district, SW China: Their relationship to the Emeishan mantle plume. *Chem. Geol.* **2007**, *243*, 286–316. [CrossRef]
7. Xu, Y.G.; Chung, S.L.; Jahn, B.M.; Wu, G.Y. Petrologic and geochemical constraints on the petrogenesis of Permian–Triassic Emeishan flood basalts in southwestern China. *Lithos* **2001**, *58*, 145–168. [CrossRef]
8. Xu, Y.G.; Luo, Z.Y.; Huang, X.L.; He, B.; Xiao, L.; Xie, L.W.; Shi, Y.R. Zircon U–Pb and Hf isotope constraints on crustal melting associated with the Emeishan mantle plume. *Geochim. Cosmochim. Acta* **2008**, *72*, 3084–3104. [CrossRef]
9. Zhong, H.; Zhu, W.G.; Hu, R.Z.; Xie, L.W.; He, D.F.; Liu, F.; Chu, Z.Y. Zircon U–Pb age and Sr–Nd–Hf isotope geochemistry of the Panzhihua A-type syenitic intrusion in the Emeishan large igneous province, southwest China and implications for growth of juvenile crust. *Lithos* **2009**, *110*, 109–128. [CrossRef]
10. Zhong, H.; Campbell, I.H.; Zhu, W.G.; Allen, C.M.; Hu, R.Z.; Xie, L.W.; He, D.F. Timing and source constraints on the relationship between mafic and felsic intrusions in the Emeishan large igneous province. *Geochim. Cosmochim. Acta* **2011**, *75*, 1374–1395. [CrossRef]
11. Zhou, M.F.; Arndt, N.T.; Malpas, J.; Wang, C.Y.; Kennedy, A.K. Two magma series and associated ore deposit types in the Permian Emeishan large igneous province, SW China. *Lithos* **2008**, *103*, 352–368. [CrossRef]
12. Wang, F.L.; Wang, Y.W.; Zhao, T.P. Boron isotopic constraints on the Nb and Ta mineralization of the syenitic dykes in the ~260 Ma Emeishan large igneous province (SW China). *Ore Geol. Rev.* **2015**, *65*, 1110–1126. [CrossRef]
13. Yin, R.; Sun, X.M.; Wang, S.W.; Wang, R.C.; Ran, M.L.; Wu, B.; Huang, X.L. Zircons in NYF-type pegmatites in the Emeishan large igneous province, SW China: A record of Nb and REE mineralization processes. *Ore Geol. Rev.* **2023**, *162*, 105700. [CrossRef]
14. Černý, P.; Ercit, T.S. The classification of granitic pegmatites revised. *Can. Mineral.* **2005**, *43*, 2005–2026. [CrossRef]
15. He, J.L. Ore-forming geological conditions and prospecting potential for Nb-Ta mineral deposits in Panzhihua-Xichang region, Sichuan. *Acta Geol. SiChuan* **2004**, *24*, 206–211, (In Chinese with English Abstract).
16. Linnen, R.L.; Keppler, H. Columbite solubility in granitic melts: Consequences for the enrichment and fractionation of Nb and Ta in the Earth's crust. *Contrib. Mineral. Petr.* **1997**, *128*, 213–227. [CrossRef]
17. McNeil, A.G.; Linnen, R.L.; Flemming, R.L. Solubility of wodginite, titanowodginite, microlite, pyrochlore, columbite-(Mn) and tantalite-(Mn) in flux-rich haplogranitic melts between 700° and 850 °C and 200 MPa. *Lithos* **2020**, *352–353*, 105239. [CrossRef]
18. Yin, R.; Huang, X.L.; Wang, R.C.; Sun, X.M.; Tang, Y.; Wang, Y.; Xu, Y.G. Rare-metal enrichment and Nb–Ta fractionation during magmatic–hydrothermal processes in rare-metal granites: Evidence from zoned micas from the Yashan pluton, South China. *J. Petrol.* **2022**, *63*, egac093. [CrossRef]

19. Tang, Y.; Linnen, R.L.; McNeil, A.G. An experimental study of pyrochlore solubility in peralkaline granitic melts. *Econ. Geol.* **2023**, *118*, 209–223.
20. Yin, R.; Huang, X.L.; Xu, Y.G.; Wang, R.C.; Wang, H.; Yuan, C.; Ma, Q.; Sun, X.M.; Chen, L.L. Mineralogical constraints on the magmatic–hydrothermal evolution of rare-elements deposits in the Bailongshan granitic pegmatites, Xinjiang, NW China. *Lithos* **2020**, *352–353*, 105208. [CrossRef]
21. Zhu, Y.X.; Wang, L.X.; Ma, C.Q.; Wiedenbeck, M.; She, Z.B. Titanite as a tracer for Nb mineralization during magmatic and hydrothermal processes: The case of Fangcheng alkaline complex, Central China. *Chem. Geol.* **2022**, *608*, 121028. [CrossRef]
22. Atencio, D.; Andrade, M.B.; Christy, A.G.; Gieré, R.; Kartashov, P.M. The pyrochlore supergroup of minerals: Nomenclature. *Can. Miner.* **2010**, *48*, 673–698. [CrossRef]
23. Lumpkin, G.R.; Ewing, R.C. Geochemical alteration of pyrochlore group minerals. pyrochlore subgroup. *Am. Miner.* **1995**, *80*, 732–743. [CrossRef]
24. Lumpkin, G.R.; Ewing, R.C.; Williams, C.T.; Mariano, A.N. An overview of the crystal chemistry, durability, and radiation damage effects of natural pyrochlore. *MRS Proc.* **2000**, *663*, 921. [CrossRef]
25. Hogarth, D.D.; Williams, C.T.; Jones, P. Primary zoning in pyrochlore group minerals from carbonatites. *Miner. Mag.* **2000**, *64*, 683–697. [CrossRef]
26. McCreath, J.A.; Finch, A.A.; Herd, D.A.; Armour, B.A. Geochemistry of pyrochlore minerals from the Motzfeldt Center, South Greenland: The mineralogy of a syenite-hosted Ta Nb deposit. *Am. Miner.* **2013**, *98*, 426–438. [CrossRef]
27. Sun, Z.H.; Qin, K.Z.; Mao, Y.J.; Tang, D.M.; Wang, F.Y.; Evans, N.J. Mineral chemistry of pyrochlore supergroup minerals from the Boziguoer Nb-Ta-Zr-Rb-REE deposit, NW China: Implications for Nb enrichment by alkaline magma differentiation. *Minerals* **2022**, *12*, 785. [CrossRef]
28. Walter, B.F.; Parsapoor, A.; Braunger, S.; Marks, M.A.W.; Wenzel, T.; Martin, M.; Markl, G. Pyrochlore as a monitor for magmatic and hydrothermal processes in carbonatites from the Kaiserstuhl volcanic complex (SW Germany). *Chem. Geol.* **2018**, *498*, 1–16. [CrossRef]
29. Wu, B.; Hu, Y.Q.; Bonnetti, C.; Xu, C.; Wang, R.C.; Zhang, Z.S.; Li, Z.Y.; Yin, R. Hydrothermal alteration of pyrochlore group minerals from the Miaoya carbonatite complex, central China and its implications for Nb mineralization. *Ore Geol. Rev.* **2021**, *132*, 104059. [CrossRef]
30. Xue, Y.; Sun, N.Y.; Li, G.W. Evolution of Nb–Ta oxide minerals and their relationship to the magmatic-hydrothermal processes of the Nb–Ta mineralized syenitic dikes in the Panxi region, SW China. *Minerals* **2022**, *11*, 1204. [CrossRef]
31. Zhou, M.F.; Yan, D.P.; Kennedy, A.K.; Li, Y.Q.; Ding, J. SHRIMP U–Pb zircon geochronological and geochemical evidence for Neoproterozoic arc-magmatism along the western margin of the Yangtze Block, South China. *Earth Planet. Sci. Lett.* **2002**, *196*, 51–67. [CrossRef]
32. Zhao, J.H.; Zhou, M.F. Neoproterozoic adakitic plutons and arc magmatism along the western margin of the Yangtze Block, South China. *J. Geol.* **2007**, *115*, 675–689. [CrossRef]
33. Yan, D.P.; Zhou, M.F.; Song, H.L.; Wang, X.W.; Malpas, J. Origin and tectonic significance of a Mesozoic multi layer over thrust system within the Yangtze Block (South China). *Tectonophysics* **2003**, *361*, 239–254. [CrossRef]
34. Song, X.Y.; Zhou, M.F.; Hou, Z.Q.; Cao, Z.M.; Wang, Y.L.; Li, Y. Geochemical constraints on the mantle source of the upper Permian Emeishan continental flood basalts, southwestern China. *Int. Geol. Rev.* **2001**, *43*, 213–225. [CrossRef]
35. Xiao, L.; Xu, Y.G.; Mei, H.J.; Zheng, Y.F.; He, B.; Pirajno, F. Distinct mantle sources of low-Ti and high-Ti basalts from the western Emeishan large igneous province, SW China: Implications for plume–lithosphere interaction. *Earth Plane. Sc. Lett.* **2004**, *228*, 525–546. [CrossRef]
36. Huang, H.; Huyskens, M.H.; Yin, Q.Z.; Cawood, P.A.; Hou, M.C.; Yang, J.H.; Xiong, F.H.; Du, Y.S.; Yang, C.C. Eruptive tempo of Emeishan large igneous province, southwestern China and northern Vietnam: Relations to biotic crises and paleoclimate changes around the Guadalupian-Lopingian boundary. *Geology* **2022**, *50*, 1083–1087. [CrossRef]
37. Shellnutt, J.G. The Emeishan large igneous province: A synthesis. *Geosci. Front.* **2014**, *5*, 369–394. [CrossRef]
38. Zhong, H.; Zhu, W.G.; Song, X.Y.; He, D.F. SHRIMP U–Pb zircon geochronology, geochemistry, and Nd–Sr isotopic study of contrasting granites in the Emeishan large igneous province, SW China. *Chem. Geol.* **2007**, *236*, 112–133. [CrossRef]
39. Munteanu, M.; Yao, Y.; Wilson, A.H.; Chunnett, G.; Luo, Y.N.; He, H.; Cioacă, M.; Wen, M.L. Panxi region (South-West China): Tectonics, magmatism and metallogenesis. A review. *Tectonophysics* **2013**, *608*, 51–71. [CrossRef]
40. Lu, P.F.; Liu, P.P. Constraints of combined Sr-Nd-Pb-Hf-O isotopic systematics on the petrogenesis of peralkaline, metaluminous and peraluminous granitoids in the Permian Emeishan large igneous province, SW China. *Chem. Geol.* **2023**, *624*, 121423. [CrossRef]
41. Hou, T.; Zhang, Z.C.; Encarnacion, J.; Santosh, M. Petrogenesis and metallogenesis of the Taihe gabbroic intrusion associated with Fe–Ti-oxide ores in the Panxi district, Emeishan Large Igneous Province, southwest China. *Ore Geol. Rev.* **2012**, *49*, 109–127. [CrossRef]
42. Zhong, H.; Yao, Y.; Prevec, S.A.; Wilson, A.H.; Viljoen, M.J.; Viljoen, R.P.; Liu, B.G.; Luo, Y.N. Trace-element and Sr–Nd isotopic geochemistry of the PGE-bearing Xinjie layered intrusion in SW China. *Chem. Geol.* **2004**, *203*, 237–252. [CrossRef]
43. Zhong, H.; Yao, Y.; Hu, S.F.; Zhou, X.H.; Liu, B.G.; Sun, M.; Zhou, M.F.; Viljoen, M.J. Trace-element and Sr-Nd isotopic geochemistry of the PGE-bearing Hongge layered intrusion, Southwestern China. *Int. Geol. Rev.* **2003**, *45*, 371–382. [CrossRef]

44. Shellnutt, J.G.; Wang, C.Y.; Zhou, M.F.; Yang, Y.H. Zircon Lu–Hf isotopic compositions of metaluminous and peralkaline A-type granitic plutons of the Emeishan large igneous province (SW China): Constraints on the mantle source. *J. Asian Earth Sci.* **2009**, *35*, 45–55. [CrossRef]
45. Zurevinski, S.E.; Mitchell, R.H. Extreme compositional variation of pyrochlore group minerals at the Oka carbonatite complex, Quebec: Evidence of magma mixing. *Can. Miner.* **2004**, *42*, 1159–1168. [CrossRef]
46. Nasraoui, M.; Bilal, E. Pyrochlores from the Lueshe carbonatite complex (Democratic Republic of Congo): A geochemical record of different alteration stages. *J. Asian Earth Sci.* **2000**, *18*, 237–251. [CrossRef]
47. Vasyukova, O.V.; Williams-Jones, A.E. A new model for the origin of pyrochlore: Evidence from the St Honor´e Carbonatite, Canada. *Chem. Geol.* **2023**, *632*, 121549. [CrossRef]
48. Ivanyuk, G.Y.; Konopleva, N.G.; Yakovenchuk, V.N.; Pakhomovsky, Y.A.; Panikorovskii, T.L.; Kalashnikov, A.O.; Bocharov, V.N.; Mikhailova, J.A.; Bazai, A.A.; Goryainov, P.M. Three-D mineralogical mapping of the Kovdor phoscorite-carbonatite complex, NW Russia: III. Pyrochlore supergroup minerals. *Minerals* **2018**, *8*, 277. [CrossRef]
49. Viladkar, S.G.; Sorokhtina, N.V. Evolution of pyrochlore in carbonatites of the Amba Dongar complex, India. *Miner. Mag.* **2021**, *85*, 554–567. [CrossRef]
50. Zaitsev, A.N.; Spratt, J.; Shtukenberg, A.G.; Zolotarev, A.A.; Britvin, S.N.; Petrov, S.V.; Kuptsova, A.V.; Antonov, A.V. Oscillatory- and sector- zoned pyrochlore from carbonatites of the Kerimasi volcano, Gregory rift, Tanzania. *Miner. Mag.* **2021**, *85*, 532–553. [CrossRef]
51. Zaitsev, A.N.; Williams, C.T.; Wall, F.; Zolotarev, A.A. Evolution of chemical composition of pyrochlore group minerals from phoscorites and carbonatites of the Khibina alkaline massif. *Geol. Ore Deposit.* **2012**, *54*, 503–515. [CrossRef]
52. Zhang, A.C.; Wang, R.C.; Hu, H.; Zhang, H.; Zhu, J.C.; Chen, X.M. Chemical evolution of Nb-Ta oxides and zircon from the Koktokay No. 3 granitic pegmatite, Altai, northwestern China. *Mineral. Mag.* **2004**, *68*, 739–756. [CrossRef]
53. Lahti, S.I. Zoning in columbite-tantalite crystals from the granitic pegmatites of the Erajarvi area, southern Finland. *Geochim. Cosmochim. Acta* **1987**, *51*, 509517. [CrossRef]
54. Černý, P.; Novak, M.; Chapman, R. Effects of sillimanite-grade metamorphism and shearing on Nb-Ta oxide minerals in granitic pegmatites: Marsikov, NorthernMoravia, Czechoslovakia. *Can. Miner.* **1992**, *30*, 699718.
55. Norton, D.L.; Dutrow, B.L. Complex behavior of magma-hydrothermal rocesses: Role of supercritical fluid. *Geochim. Cosmochim. Acta* **2001**, *65*, 4009–4017. [CrossRef]
56. Stepanov, S.; Mavrogenes, J.A.; Meffre, S.; Davidson, P. The key role of mica during igneous concentration of tantalum. *Contrib. Mineral. Petr.* **2014**, *169*, 1009. [CrossRef]
57. Wark, D.A.; Miller, C.F. Accessory mineral behavior during differentiation of a granitic suite: Monazite, xenotime, and zircon in the Sweetwater Wash pluton, southeastern California, U.S.A. *Chem. Geol.* **1993**, *110*, 49–67. [CrossRef]
58. Linnen, R.L.; Cuney, M. Granite-related rare-element deposits and experimental constraints on Ta-Nb-W-Sn-Zr-Hf mineralization. In *Rare-Element Geochemistry and Mineral Deposits*; Linnen, R.L., Samson, I.M., Eds.; Geological Association of Canada Short Course Notes; Geological Association of Canada: St. John's, NL, Canada, 2005; Volume 17, pp. 70–102.
59. Bartels, A.; Vetere, F.; Holtz, F.; Behrens, H.; Linnen, R.L. Viscosity of flux-rich pegmatitic melts. Contrib. *Mineral. Petrol.* **2011**, *162*, 51–60. [CrossRef]
60. London, D. Internal differentiation of rare-element pegmatites: Effects of boron, phosphorus, and fluorine. *Geochim. Cosmochim. Acta* **1987**, *51*, 403–420. [CrossRef]
61. London, D.; George, B.M., VI; Babb, H.A.; Loomis, J.L. Behavior and effects of phosphorus in the system Na_2O-K_2O-Al_2O_3-SiO_2-P_2O_5-H_2O at 200 MPa(H_2O). Contrib. *Mineral. Petr.* **1993**, *113*, 450–465. [CrossRef]
62. Anderson, A.J.; Mayanovic, R.A.; Lee, T. The Local Structure of Ta(v) Aqua ions in high temperature fluoride- and chloride-bearing solutions: Implications for Ta transport in granite-related postmagmatic fluids. *Can. Mineral.* **2019**, *57*, 843–851. [CrossRef]
63. Timofeev, A.; Migdisov, A.A.; Williams-Jones, A.E. An experimental study of the solubility and speciation of tantalum in fluoride-bearing aqueous solutions at elevated temperature. *Geochim. Cosmochim. Acta* **2017**, *197*, 294–304. [CrossRef]
64. Zaraisky, G.P.; Korzhinskaya, V.; Kotova, N. Experimental studies of Ta_2O_5 and columbite–tantalite solubility in fluoride solutions from 300 to 550 °C and 50 to 100 MPa. *Miner. and Petrol.* **2010**, *99*, 287–300. [CrossRef]

Disclaimer/Publisher's Note: The statements, opinions and data contained in all publications are solely those of the individual author(s) and contributor(s) and not of MDPI and/or the editor(s). MDPI and/or the editor(s) disclaim responsibility for any injury to people or property resulting from any ideas, methods, instructions or products referred to in the content.